Magnetocaloric properties at the austenitic Curie transition in Cu and Fe substituted Ni-Mn-In Heusler compounds


# Magnetocaloric properties at the austenitic Curie transition in Cu and Fe substituted Ni-Mn-In Heusler compounds

Simone Fabbrici, Francesco Cugini, Fabio Orlandi, Nicola Sarzi Amadè, Francesca Casoli, Davide Calestani, Riccardo Cabassi, Greta Cavazzini, Lara Righi, Massimo Solzi, Franca Albertini

PII: S0925-8388(21)04659-4

DOI: https://doi.org/10.1016/j.jallcom.2021.163249

Reference: JALCOM163249

To appear in: *Journal of Alloys and Compounds*

Received date: 12 October 2021
Revised date: 8 December 2021
Accepted date: 11 December 2021

Please cite this article as: Simone Fabbrici, Francesco Cugini, Fabio Orlandi, Nicola Sarzi Amadè, Francesca Casoli, Davide Calestani, Riccardo Cabassi, Greta Cavazzini, Lara Righi, Massimo Solzi and Franca Albertini, Magnetocaloric properties at the austenitic Curie transition in Cu and Fe substituted Ni-Mn-In Heusler compounds, *Journal of Alloys and Compounds,* (2021) doi:https://doi.org/10.1016/j.jallcom.2021.163249

# Magnetocaloric properties at the austenitic Curie transition in Cu and Fe substituted Ni-Mn-In Heusler compounds

Simone Fabbrici[a,b *], Francesco Cugini[a,c], Fabio Orlandi[d], Nicola Sarzi Amadè[a,c], Francesca Casoli[a], Davide Calestani[a], Riccardo Cabassi[a], Greta Cavazzini[a,c], Lara Righi[a,e], Massimo Solzi[a,c], and Franca Albertini[a]

[a] Institute of Materials for Electronics and Magnetism, National Research Council (IMEM-CNR), Parco Area delle Scienze 37/A, I-43124 Parma, Italy
[b] MISTER Laboratory, v. P. Gobetti 101, I-40129 Bologna, Italy
[c] Department of Mathematical, Physical and Computer Sciences, University of Parma, Parco Area delle Scienze 7/A I-43124 Parma, Italy.
[d] ISIS Pulsed Neutron Facility, STFC, Rutherford Appleton Laboratory, Chilton, Didcot, Oxfordshire OX11-0QX, United Kingdom
[e] Department of Chemistry, Life Sciences and Environmental Sustainability, University of Parma, Parco Area delle Scienze 17/A I-43124 Parma, Italy.
[*] corresponding author: simone.fabbrici@imem.cnr.it

**Abstract**

We present a study on the Curie transition of austenitic Ni-Mn-In full Heusler compounds when Mn atoms are replaced by Fe or Cu. The substituted compounds are designed to present a relevant magnetocaloric effect at the second order Curie transition of the austenitic phase near room temperature. We show that Fe and Cu modify the magnetic moments and interactions responsible of the localized magnetism in the $L2_1$ ordered cubic structure, resulting in a change of the Curie temperature and saturation magnetization of the compound. Neutron diffraction experiments and electron microscopy analysis were used to study the sites occupancy of doping atoms and the presence of secondary phases, thus possibly optimizing the annealing protocols to obtain homogeneous samples even at high Cu/Fe concentrations. On this basis, a series of quinary compounds with a tunable Curie temperature and high values of saturation magnetization (100-110 $Am^2/Kg$ at 80 K) was successfully synthesized. The obtained results show the feasible fine tuning of the Curie temperature at which the peak of the magnetocaloric effect is realized, highlighting a new promising strategy to design graded regenerators for room temperature magnetocaloric applications.

**Keywords**: heusler alloys, Ni-Mn-In, magnetocaloric effect, neutron diffraction

## Introduction

$Ni_{50}Mn_{25+x}In_{25-x}$ full Heusler alloys, belonging to the vast class of intermetallic Ni-Mn-based Heusler compounds [1,2], are intensively investigated from both theoretical and experimental points of view for the great variety of functional properties related to a magneto-structural martensitic transformation from a high-temperature ferromagnetic austenitic phase to a low-temperature weak-magnetic martensitic phase [3–5]. The large magnetization change between the two phases gives rise to technologically relevant

properties in sensing/actuation and magnetic refrigeration applications, such as magnetic field induced strain [6], giant magnetoresistance [7] and large inverse magnetocaloric effects (MCE) [8].

Promising results concerning the magnetocaloric applications are achievable if the magneto-structural transition temperature ($T_M$) occurs at around room temperature and the associated magnetization change is large and reversible under thermo-magnetic cycles in suitable external magnetic field (i.e. magnetic fields lower than 2 Tesla, which are achievable with permanent magnets) [9–12]. In fact, a large magnetization jump allows an increased sensitivity of the critical temperatures to the applied magnetic fields and a sizeable improvement of the magnetic entropy change [13].

Several strategies have been studied to tailor the critical temperatures and to enhance the magnetocaloric effect in these compounds. First, it is possible to tune $T_M$ by controlling the compound stoichiometry [13-15] allowing, for instance, the co-occurrence of the structural and magnetic transitions accompanied by a significant magnetization change, as in the case of $Ni_2MnGa$ [16]. Secondly, the magnetization jump across the magneto-structural transition can be increased by changing the magnetic interactions of the two structural phases [17], so that in the vicinity of the transformation one phase has negligible magnetization, while the other carries a far higher magnetic moment.

This has been achieved tuning the composition by several approaches: i) modifying the number and size of atomic moments contributing to the total magnetization [18–20]; ii) varying the lattice constant by selecting iso-electronic elements with different atomic radii [21]; iii) altering the interatomic distances between the Mn atoms carrying the magnetic moment [22–25]; and/or iv) changing the electronic band structure, by the substitutional methods [14,26–29].

Most of the literature focuses on Heusler compounds with large discontinuities at the magneto-structural transition, since they enable a giant magnetocaloric effect ($\Delta T_{ad}$) with peak values much higher than the benchmark magnetocaloric material, Gadolinium [8,11]. Unfortunately, due to the large thermal hysteresis of the first order magneto-structural transformation [30–34], the reversibility of such outstanding MCE is hindered and drastically reduced after the first cycle [11,33], as well as the effective working temperature range, which is eventually lower than Gd [32,35]. Moreover, in first order magnetostructural transitions the effective magnetocaloric performance is also heavily dependent on the applied field. While the majority of literature data is provided for a magnetic field change of 2 Tesla, which is considered as the maximum magnetic field change achievable with permanent magnets, in reality most magnetocaloric devices operate with magnetic field changes lower than such limit. In [36] the cyclability of the MCE is tested in both 2 T and 1 T magnetic field changes: the Heusler compound Ni-Co-Mn-In, which shows [11] considerable $\Delta T_{ad}$ peak values of 8 K (irreversible) and 3K (reversible) in a 2 T field change, shows on the other hand a negligible reversible MCE ($\Delta T_{ad}$ less than 0.3 K) in a 1 T field change.

A far less exploited approach in the magnetocaloric Heusler compounds is the maximization of the magnetization change near the second order Curie transition of the austenite, which has the benefit of being inherently reversible, thus possibly overcoming all the drawbacks shown by the magneto-structural transformation. Second order austenitic Heulser compounds are particularly interesting as they are rare-earth free, easy to synthesize also above the typical laboratory scale (up to 250 grams [10]) and show unique tailoring capabilities.

The ternary $Ni_{49}Mn_{35}In_{16}$ compound has emerged [37] as a good candidate for the fully reversible MCE exploitable in room-temperature magnetic refrigeration technology. In fact, a full stabilization of the ferromagnetic austenite within the entire temperature range is realized, showing both a high saturation magnetization ($M_s \approx 6\ \mu_B$/f.u., circa 125 $Am^2$/Kg) and a Curie temperature slightly higher than room temperature ($T_c$ = 316 K). In addition, a maximum adiabatic temperature change of $\Delta T_{ad} \approx 1.5$ K/T has been reported [37]: such value represents a consistent fraction of the maximum temperature change of Gadolinium, which is reported in the literature between 2 and 2.8 K in 1 T field [36, 37]. However, the tuneability of the Curie transition closer to room temperature in the Mn-rich Ni-Mn-In series is still missing and required to actually exploit these materials in technological devices, for an alternative green magnetic refrigeration solution [15,36].

Very recently, theoretical studies on a closely related series such as the Ni-Mn-Sb Heusler compounds have suggested the chemical co-substitution as a mean to drive the Curie transition close to room temperature for magnetocaloric purposes. [38]. Therefore, an experimental validation of such results is now required.

Focusing on Ni-Mn-In Heusler compounds, different published works have investigated the effects of Fe and Cu doping on the magnetic, structural, and magnetocaloric properties of the samples [24,27,39–46]. However, the magnetocaloric performance has been assessed around the martensitic transformation, while at the Curie transition has been overlooked.

The main goal of the present work is the achievement of a fine control of the Curie transition temperature in samples with the austenitic phase, while preserving a large and reversible magnetocaloric response Ni-Mn-In-based Heusler compounds.

Starting from $Ni_{50-x}Mn_{34+x}In_{16}$ composition, we investigated:

(i) ternary compounds by varying the Mn over Ni ratio;

(ii) quaternary compounds with different Mn-substitutions by Cu, expected to reduce the magnetic interactions;

(iii) quaternary compounds with Mn-replaced by Fe, expected to enhance the total magnetic moment;

(iv) quinary compounds by combining suitable Fe and Cu substitutions for Mn.

Magnetometry and direct MCE measurements at the Curie transition have been performed to assess

the magnetic and magnetocaloric properties of the prepared compounds, whereas neutron diffraction experiments have been carried out to determine the preferential doping sites for Fe and Cu.
In this study we obtained the stabilization of the austenitic phase down to the lowest temperatures for all the explored compositions and the fine tuning of the Curie temperature in a range of interest for room temperature magnetocaloric applications.

**Experimental**

By fixing the In content, four series of compounds with nominal composition $(Ni,Mn,Fe,Cu)_{84}In_{16}$ were obtained and investigated by changing the ratio of (i) Mn over Ni, (ii) Cu over Mn, (iii) Fe over Mn and (iv) Cu and Fe over Mn, namely:
(i) $Ni_{50-x}Mn_{34+x}In_{16}$: Mn(Ni) series;
(ii) $Ni_{48}Mn_{36-y}Cu_yIn_{16}$: Cu(Mn) series;
(iii) $Ni_{48}Mn_{36-z}Fe_zIn_{16}$: Fe(Mn) series;
(iv) $Ni_{48}Mn_{36-y-z}Cu_yFe_zIn_{16}$: Cu-Fe(Mn) series.

All the polycrystalline samples were prepared from high-purity elements by arc melting under a protective Ar atmosphere. The ingots were re-melted several times (up to four times) before being homogenized at different annealing temperatures (ranging between 1073 and 1173 K) in high purity Ar atmosphere. The compositions of the samples were analyzed by energy dispersive X-ray spectroscopy (EDS) in a scanning electron microscope (Bruker Esprit microanalysis on a FEG-ESEM FEI QUANTA 250). Small samples for thermo-magnetic measurements were obtained from a disk previously cut from the ingots with a slow-speed diamond saw. The thermo-magnetic curves, used to determine the critical temperatures, $T_M$ and Tc, were obtained by a.c. susceptibility measurements in low applied magnetic field (10 Oe) as a function of temperature. The a.c. susceptibility plots were normalized to unity in order to better compare the critical temperatures of the different samples. Magnetic measurements were carried out by using extraction magnetometry (MagLab System2000 by Oxford Instrument). The reversible adiabatic temperature change $\Delta T_{ad}$ was measured directly with a Cernox based probe [47] with a 1.0 T magnetic field cyclically applied to the sample.
Insight on atomic site occupancy of Fe and Cu substituted compounds was obtained through Rietveld refinement of time-of-flight neutron diffraction data obtained at the ISIS facility (UK) on the WISH diffractometer [48]; the measurements were collected above the Curie temperature of the samples to exclude magnetic contributions and were fitted through Rietveld refinement with the JANA2006 software [49]. The powder samples were obtained by hand grinding in a mortar and subsequently heat treated at low temperature (773 K for 4 hours) to relieve the mechanical stress introduced during the preparation.

The samples were contained in a 3 mm thin wall vanadium can to minimize neutron absorption mainly due to In. The refinements were conducted on the WISH detector banks with average 2-θ of 152.8, 121.6, 90 and 58.2 degrees each covering 32 degrees of the scattering plane. The sample absorption was corrected during the refinement with an empirical exponential law. To avoid unwanted correlation with the site occupancies, the atomic thermal parameters of the atoms in the structure were constrained to the same value.

**Results and Discussion**

The $Ni_{50-x}Mn_{34+x}In_{16}$ series was designed to keep an almost fixed In content while varying the Ni/Mn ratio. By increasing the amount of Mn, the number of atoms with high magnetic moment per unit cell was increased, while the austenitic phase was stabilized by suppressing the structural transformation. After the melting, the obtained ternary ingots were annealed at 1073 K for 72 h and rapidly quenched in water. The annealing temperature was selected above the order/disorder transition of the In <16 at% compound according to Miyamoto et. al. [50], to promote a high atomic mobility and, hence, homogeneity. Figure 1 reports the normalized low field a.c. susceptibility measurements of the Ni(Mn) series as a function of the Mn content. Table I reports the measured compositions, the critical temperatures and the saturation magnetization measured at low temperature (at 80 K).

The reference composition of this series, sample x=0, shows both Curie temperature and magneto-structural transformation. A comprehensive analysis of the magnetocaloric properties at the first order transformation is reported in Ref. [51]. It is observed that, starting from a composition where the martensitic and Curie transitions co-occur (x = -2), $T_M$ decreases with x. The Curie transition for sample x=-2 is not visible in the susceptibility measurement and it is extrapolated from the Arrott plots (Table I). On Mn increasing, the structural transition is suppressed already at $x \geq 1$ and the values of saturation magnetization measured at 80 K, in 1 Tesla field, $M_s$(80 K), reveal a peak at Mn ≈ 35 at% despite an almost constant $T_c$. Previous studies [52] have observed that increasing Mn in place of In, from 25 to 35 at%, allows increasing $M_s$, while for Mn > 35 at %, the rise of the martensitic transformation temperature above the austenitic Curie transition prevents the onset of the ferromagnetic order in the austenite. In our case, as far as we increase Mn in place of Ni, we stabilize the ferromagnetic austenite up to Mn = 40 at % (x=6), but we also slightly lower its magnetization (down by 4%, see Table I). To understand such behavior, we consider the Mn = 36 at% (x = 2) sample of the series. The XRD pattern in Figure 2(a) confirms the austenitic structure at room temperature, with lattice parameter, calculated by a simple le Bail fitting of the peaks positions, of 6.02±0.01 Å. The presence of the (111), (311) and (331) reflections, typical of the $L2_1$ superstructure [53], indicates also some degree of atomic ordering in the Mn and In sublattices. The

expected atomic configuration is sketched in Figure 2(b). The excess of Mn atoms (x = 2) in the Ni site gives rise to an additional group of Mn-Mn distances (Mn-Ni = 2.61 Å) which are shorter than that in the $Ni_{50}$-type compound (Mn-In and Mn-Mn distances being respectively ≈ 3.01 and 4.25 Å) [1,17]. Since the direct exchange integral between manganese atoms is usually antiferromagnetic below 2.9 Å [54], the decrease of $M_s$ with x can be explained by the appearance of Mn-Mn antiferromagnetic interactions which are on the other hand absent in the x=0 compound.

Since we were interested in samples with no martensitic instability near room temperature, we considered the x=2 sample ($Ni_{48.1}Mn_{34.7}In_{17.2}$) as representative to study the role of substitutional Cu and Fe atoms on the magnetic properties. As reported in Figure 2(c), it shows only the ferromagnetic second order transition with a large saturation magnetization value (≈ 125 $Am^2/Kg$) of the cubic austenitic phase.

Aimed at decreasing its Tc (314.9 K) towards room temperature while keeping the high magnetic moment of the austenite unchanged, we investigated, as a first step, the effects of a gradual replacement of Mn by Cu (series Cu(Mn)) or by Fe (series Fe(Mn)). It is expected that Cu, being non-magnetic, will dilute the magnetic interactions in the lattice; Fe, on the contrary, will carry additional magnetic moment in the full Heusler system.

The elemental analysis of the obtained samples is reported in Table II, while Figure 3 shows the low-field thermo-magnetic analysis of the substituted compounds, annealed under the same conditions as the ternary series, i.e. at 1073 K.

Depending on the element introduced into the ternary compound, different trends can be observed. In the Cu(Mn) series, the Curie temperature of the compounds gradually decreases towards and below room temperature on increasing the amount of Cu. In the Fe(Mn) series the opposite occurs, as the Curie temperature increases with the content of Fe. The doping element is incorporated in the Heusler phase up to a certain amount: in fact, a single Curie transition is found for the compounds with Fe or Cu substitution up to 4 at % or 6 at%, respectively. At higher substitution percentages we observe some peculiarity in both series: the susceptibility measure for Fe10 sample shows (Fig. 4c) a double slope in the proximity of the Curie temperature, which suggests the presence of two or more magnetic phases. Similarly, the magnetic transition of the Cu8 sample (Fig. 4f) does not show a single and well-defined slope at $T_C$, but rather a main transition temperature with broad tails and minor kinks at both higher and lower temperatures. Additionally, the $T_C$ of the Cu8 sample deviates from the trend outlined by the other samples of the Cu(Mn) series.

Back scattering electrons images, performed on both Cu8 and Fe10 samples, clearly reveal secondary phases as shown in Figure 4(a) and 4(d). The secondary phases (darker areas in the 4a and 4d SEM back scattering maps) are elemental Fe inclusions in the Fe-substituted sample and $Ni_{52.6}Mn_{27.7}In_{3.8}Cu_{15.9}$ for the Cu-substituted one. The latter phase is an In-poor pseudo-binary compound which has been already

reported in disproportioned Heusler compounds [55]. It is expected to have a tetragonal structure and weak magnetic signal due to the underlying antiferromagnetic long-range order.

These two samples, Fe10 and Cu8, were selected for an additional post annealing to test if treatment at higher temperatures would improve the solubility of the doping elements into the main phase. Two pieces extracted from the ingots were treated at 1173 K for 24 hours and then water quenched and compared to the original ingots homogenized at 1073 K. The volume of the secondary phase precipitates decreases drastically in the case of Fe- and completely disappears in the case of Cu-substitution after the additional heat treatment at 1173 K, as testified by Figs. 4(b) and4(e).

The Curie temperatures of the austenite phases, also reported in Figs. 4c and 4f, mirror these micro structural and metallurgical features. In Fe-substituted samples, as the secondary phase precipitates become smaller and mainly appear at the grain boundaries (Figure 4(b)), a unique Curie temperature is observed in the magnetization measurements reported in Figure 4(c). In the case of the Cu= 8 at%, the high-temperature annealing treatment allows to restore the trend expected along the Cu(Mn) series for the austenitic Tc, which passes from 288.7 K for the sample homogenized at 1073 K, to 271 K for the post annealed sample, as displayed in Figure 4(f).

$T_c$, $M_s$(80 K) and the main phase elemental compositions after each heat treatment are summarized in Table II. It appears evident that the high atomic diffusivity reachable close to the melting point of the samples promotes the desired (nominal) stoichiometry and improves the phase homogeneity even at high substitution percentages of Fe or Cu. We still observe a solid solubility limit for Fe, above which we observe iron precipitates. However, differently from previous limits of about 3 and 4 % for iron in $Ni_{50}Mn_{40-x}Sn_{10}Fe_x$ reported in [56,57] and $Ni_{50}Mn_{36}In_{16-x}Fe_x$ [39], we demonstrate a greater amount of iron in the main Heusler phase (almost 6 %) which is promoted by the high temperature homogenization step.

The different effects on the magnetic properties observed in both Cu(Mn) and Fe(Mn) series, as well as the possibility to perform large atomic substitutions, are promising to tailor $T_C$ towards room temperature without losing the large ground state magnetization showed by the ternary $Ni_{48.1}Mn_{34.7}In_{17.2}$ compound at its Curie transition temperature (i.e. at T=314.9 K). We produced for this purpose a series of quinary compounds (the Cu-Fe(Mn) series) where both Fe and Cu substitute Mn.

Table 3 shows the measured critical temperatures and chemical compositions of such quinary compounds, pointing out that the main features induced by Cu and Fe substitutions are now co-occurrent. A fine control of $T_c$ it is achieved in the samples homogenized at 1173 K as well as in those heat treated at 1073 K. The magnetic transitions of the Cu-Fe(Mn) series lie, indeed, between 290 and 299 K values which are of great interest for room temperature magnetocaloric applications. Also, it is found that the $M_S$ values of the quinary samples show slightly higher values with respect to the Cu substituted series when compared with samples containing the same amount of Mn. Figure 5 shows the measured $T_C$ and $M_s$ for all the four series of samples studied in this work as a function of the Mn content. Assuming the In content almost constant (≈

16-18 %), it can be noted that by replacing Mn with a non-magnetic element a decrease of $T_C$ and $M_s$ in all the Mn(Cu) series is obtained. The opposite trend occurs when doping with Fe, as shown by the Fe(Mn) series. Quantitatively, $M_s$ decreases of about 5.3 $Am^2/Kg$ (i.e. 0.24 $\mu_B$/f.u.) per at% of Cu on Mn; this value is close to the one due to the extra Mn atoms at the In sites for the ternary compound [52]. On the other hand, differently to what happens in ternary compounds when In replaces Mn, it is now possible to reduce the Curie temperatures towards room temperature in Cu-substituted samples.

To confirm the preferred dopant substitution site, we performed time-of-flight neutron diffraction experiments on two representative samples of both Cu(Mn) and Fe(Mn) series, samples Cu5 and Fe5, taking advantage of the different scattering length of the elements ($b_{Ni}$=10.3fm, $b_{Mn}$=-3.73fm $b_{In}$~4 fm, $b_{Fe}$=9.45 fm and $b_{Cu}$=7.718 fm). The measurement here presented were collected well above Tc for both compositions to ensure that only the atomic structure contributed to the diffraction pattern. The Cu5 Rietveld refinements, displayed in the top panel of Figure 6, produced a very good agreement with the experimental data (wRp=4.70). The main phase is austenite (space group Fm-3m) with cell parameter a= 6.00318(17)Å. The refined composition $Ni_{50.00(7)}Mn_{31.17(5)}In_{14.74(2)}Cu_{4.04(5)}$ is close to the targeted one and comparable with the EDX analysis. A very little amount of spurious phases is found: metallic Cu 0.566(14)%, NiMn alloy (likely related to the observed $Ni_{52.6}Mn_{27.7}In_{3.8}Cu_{15.9}$ phase in the SEM measurement) 0.497(11)% and MnO 0.566(18)% in mass. In the Heusler phase, the Cu atoms are found to preferentially occupy both the *4b* Mn sites and the *4a* In sites with respectively the 1.770(16) and the 2.27(3) (defined with respect to the total composition). This specific aspect, together with other considerations involving the changes in the electronic bands [58–60], may explain the different behavior of the Curie temperature induced by Cu when comparing this series with ternary compounds having the same amount of Mn. The Rietveld plot of the Fe5 sample is reported in the bottom panel of Figure 6, showing, also in this case, a good agreement between observed and calculated data (wRp=4.65%). Contrary to the previous case, the refined composition, $Ni_{43(2)}Mn_{31.46(6)}In_{18.25(3)}Fe_{7(2)}$ shows a clear reduction of the Ni content of the compound respect to the targeted composition. The missing Ni is found in the small amount of impurities observed in the diffraction data: $Ni_{0.8}In_{0.2}$ 2.12(1)%, Ni 0.487(2)%, Fe 1.393(2)% and MnO 0.215(2)%. The Fe ions occupy the Ni sites (7(2)%) and only a minimum amount (0.29(3)%) is found on the 4b Mn site. The preferential occupancy of the Fe on the Ni sites is in clear contrast with the expected tendency to occupy the 4a Mn sites as reported in literature [60], but it will still influence the magnetic properties since short Mn-Fe bond (~2.608 Å) are formed. Figure 5 reveals indeed that iron is able to increase $T_c$ and $M_s$ (+0.77 $Am^2/Kg$ (i.e. +0.09 $\mu_B$/f.u.) per at% of Fe) by modifying the magnetic interactions. Nonetheless, this effect is dependent on concentration: it is important to remark that addition of iron beyond 4% decreases the $M_S$ (Table 2).

The reversible adiabatic temperature change across the four series was measured by direct method in 1.0 T magnetic field by following the “cyclic protocol” described in [61]. Results on the selected samples are plotted in Figure 7 and demonstrate that the MCE can be effectively tuned across room temperature. It has

to be underlined that with the introduction of Fe and Cu the maximum $\Delta T_{ad}$ values are reduced compared to the ternary reference sample, yet they are consistently higher than the reversible $\Delta T_{ad}$ reported at the same field change for the martensitic NiCoMnIn compound [36]. For instance, in the quinary Fe6Cu2 sample, which has $T_C$ = 299 K, we measured a $\Delta T_{ad}$ maximum of 0.78 K in 1 T. Several aspects concur to this outcome.

First, such lowered MCE, compared to the one of $Ni_{48.1}Mn_{34.7}In_{17.2}$ sample ($\Delta T_{ad}$ maximum = 1 K in 1 T at 314.9 K), can be partially explained by the reduced $M_s$. In the region of the magnetic phase transitions, the temperature change, due to the variation of a magnetic field under adiabatic and isobaric conditions, is described [62] by

$$\Delta T(T,H) \cong -\frac{T}{C_{p,H}(H,T)} \int_{H_1}^{H_2} \left(\frac{\partial M}{\partial T}\right)_H dH \qquad (1)$$

Due to the similar specific heat, $c_p$, characterizing our samples, as far as the transition temperature and the magnetization reduce, we expect a lower MCE. In fact, in the quinary series presented in this work, the main impact on the maximum $\Delta T_{ad}$ (in the range 0.58 up to 0.82 K, see table III) is determined by the saturation magnetization $M_s$ (80K), rather than the variation in the Curie temperature (between 290 and 299 K). This trend is shown in Figure 8, where samples with similar $T_C$ present different $\Delta T_{ad}$ values due to the change of $M_S$. This feature is of interest for the development of graded regenerators.

Another very important factor that must be studied in greater detail is the sample homogeneity, which is expected to affect the sharpness of the transition, i.e. dM/dT. Inhomogeneities of Heusler compounds at the nanoscale, for instance, can give rise to phenomena such as shell ferromagnetism and pinning of spins at grain boundary [55,56]. Furthermore, especially in compounds designed out of stoichiometry, the random distribution of atoms influences the degree of atomic order allowed in the $L2_1$ structure [31,63]. In the present work we have shown by combining the neutron diffraction results with the EDX measurements, that small amounts of secondary phases could arise depending both on the type and on the amount of the substituting element introduced. Therefore, a proper heat treatment protocol must be implemented to minimize such phases. This approach has been recently employed to tune by heat treatments the magneto structural phase transitions and related magnetic properties in several promising Heusler materials such as the off-stoichiometric $Ni_2MnIn$ and $(Ni,Co)_2MnIn$ compounds [15,64–66].

However, due to the complexity of magnetic interactions characterizing full Heusler compounds, further specific investigations are required to prove the role of atomic order in our substituted compounds. It is plausible that the different MCE and $M_s$ values, encountered in our samples at constant $T_c$, depend on the degree of atomic order.

Here, we demonstrated the possibility to obtain magnetic phase transition at room temperature in off-stoichiometric Ni-Mn-In compounds by partial substitutions of Mn by Fe and Cu. The magnetic properties

of the presented quinary samples can be improved by a proper preparation route, but they also deserve a deeper investigation on the magnetic interactions established among the different sublattices.

**Conclusions**

The fine control the ferromagnetic-paramagnetic phase transition temperature of the austenitic phase in $Ni_2MnIn$ based compounds has been successfully achieved by synthesizing ternary, quaternary, and quinary off-stoichiometric compounds.

We observed that small changes in the Ni/Mn ratio can drive the martensitic transition well below room temperature for increasing Mn content. This is related to the decreasing e/a ratio and the corresponding stability conditions for the two crystallographic phases.

Doping with Fe and Cu affected the magnetic properties as follows: the introduction of Fe atoms allows an overall strengthening of the magnetic interactions, thus promoting the ferromagnetic alignment of the moments of the nearest neighboring atoms and resulting in increased $M_S$ and $T_C$. On the contrary, the introduction of Cu, which is a non-magnetic species, lowers the magnetization and the Curie temperature of the austenitic phase, due to a dilution of the magnetic sublattices. Neutron diffraction measurement allowed us to show that Cu preferentially substitute the Mn atoms in the 4a and 4b Wyckoff position whereas Fe prefers to substitute Ni in the 8c position.

The presented series of compounds, characterized by finely tunable Curie temperatures around room temperature and high saturation magnetization values, demonstrate the possibility to tailor the ferromagnetic-paramagnetic transition of $Ni_2MnIn$ compounds by using non-critical elements. This opens the route for second order phase transitions in Heusler compounds with high magnetic moment (up to 5.4 $\mu_B$/f.u. or 113 $Am^2/Kg$) at room temperature and easily tunable working temperatures, possibly exploitable in graded regenerators for magnetic refrigeration applications. Our study also highlights some critical issues when substituting atoms in $Ni_2Mn$-based Heusler compounds, as for instance a lower $\Delta T_{ad}$ than expected. This unwanted outcome on the quinary compounds is likely due to residual disorder and inhomogeneity that was not completely removed by adjusting the annealing protocols, as on the other hand has been demonstrated for the quaternary series containing Fe. A further optimization of phase homogeneity, atomic order, and microstructure are required to maximize the potential of these compounds around their second order transition.

The adiabatic temperature change values measured in this work appear still a bit lower than other magnetocaloric materials exploiting reversible transitions and tested in applications, such as Gadolinium or LaFeSi alloys ($\Delta T_{ad}$ values around 2-2.8 K/T for Gd [36,37], 1.5-2 K/T for LaFeSi compounds [67]). On the other hand, Heusler compounds remain worth studying thanks to their tailoring capabilities that promise

further optimization potential, as well for the possibility to successfully synthesize promising magnetocaloric materials without the need for critical elements such as rare earths.

**Acknowledgements**

The authors thank dr. Cecilia Bennati for her contributions on synthesis and characterization of the samples. This work has been supported by the FRIMAG project, funded by Emilia Romagna region within the 2014-20 POR-FESR program (CUP E32F16000190007). The authors acknowledge the Science and Technology Facility Council (UK) for provision of neutron beam time on the WISH diffractometer under the proposal RB1820515.

**Data availability statement**

The data that support the findings of this study are available from the corresponding author upon reasonable request.

**References**

[1] M. Acet, L. Mañosa, A. Planes, Magnetic-Field-Induced Effects in Martensitic Heusler-Based Magnetic Shape Memory Alloys, in: Handb. Magn. Mater., 2011. https://doi.org/10.1016/B978-0-444-53780-5.00004-1.

[2] A. Planes, L. Mãosa, M. Acet, Magnetocaloric effect and its relation to shape-memory properties in ferromagnetic Heusler alloys, J. Phys. Condens. Matter. (2009). https://doi.org/10.1088/0953-8984/21/23/233201.

[3] R. Kainuma, W. Ito, R.Y. Umetsu, V. V. Khovaylo, T. Kanomata, Metamagnetic shape memory effect and magnetic properties of Ni-Mn based Heusler alloys, Mater. Sci. Forum. 684 (2011). https://doi.org/10.4028/www.scientific.net/MSF.684.139.

[4] W. Ito, Y. Imano, R. Kainuma, Y. Sutou, K. Oikawa, K. Ishida, Martensitic and magnetic transformation behaviors in Heusler-type NiMnIn and NiCoMnIn metamagnetic shape memory alloys, in: Metall. Mater. Trans. A Phys. Metall. Mater. Sci., 2007. https://doi.org/10.1007/s11661-007-9094-9.

[5] Y. Sutou, Y. Imano, N. Koeda, T. Omori, R. Kainuma, K. Ishida, K. Oikawa, Magnetic and martensitic transformations of NiMnX(X=In, Sn, Sb) ferromagnetic shape memory alloys, in: Appl. Phys. Lett., 2004. https://doi.org/10.1063/1.1808879.

[6] R. Kainuma, Y. Imano, W. Ito, Y. Sutou, H. Morito, S. Okamoto, O. Kitakami, K. Oikawa, A. Fujita, T. Kanomata, K. Ishida, Magnetic-field-induced shape recovery by reverse phase transformation, Nature. 439 (2006). https://doi.org/10.1038/nature04493.

[7] V.K. Sharma, M.K. Chattopadhyay, K.H.B. Shaeb, A. Chouhan, S.B. Roy, Large magnetoresistance in Ni50Mn34In16 alloy, Appl. Phys. Lett. (2006). https://doi.org/10.1063/1.2399365.

[8] J. Liu, T. Gottschall, K.P. Skokov, J.D. Moore, O. Gutfleisch, Giant magnetocaloric effect driven by structural transitions, Nat. Mater. (2012). https://doi.org/10.1038/nmat3334.

[9] A. Taubel, T. Gottschall, M. Fries, S. Riegg, C. Soon, K.P. Skokov, O. Gutfleisch, A Comparative Study on the Magnetocaloric Properties of Ni-Mn-X(-Co) Heusler Alloys, Phys. Status Solidi Basic Res. (2018). https://doi.org/10.1002/pssb.201700331.

[10] F. Puglielli, V. Mussi, F. Cugini, N. Sarzi Amadè, M. Solzi, C. Bennati, S. Fabbrici, F. Albertini, Scale-Up of Magnetocaloric NiCoMnIn Heuslers by Powder Metallurgy for Room Temperature Magnetic Refrigeration, Front. Energy Res. (2020). https://doi.org/10.3389/fenrg.2019.00150.

[11] T. Gottschall, K.P. Skokov, B. Frincu, O. Gutfleisch, Large reversible magnetocaloric effect in Ni-Mn-In-Co, Appl. Phys. Lett. (2015). https://doi.org/10.1063/1.4905371.

[12] J. Lyubina, K. Nenkov, L. Schultz, O. Gutfleisch, Multiple metamagnetic transitions in the magnetic refrigerant La(Fe,Si)13Hx, Phys. Rev. Lett. (2008). https://doi.org/10.1103/PhysRevLett.101.177203.

[13] T. Gottschall, K.P. Skokov, D. Benke, M.E. Gruner, O. Gutfleisch, Contradictory role of the magnetic contribution in inverse magnetocaloric Heusler materials, Phys. Rev. B. (2016). https://doi.org/10.1103/PhysRevB.93.184431.

[14] G. Cavazzini, F. Cugini, M.E. Gruner, C. Bennati, L. Righi, S. Fabbrici, F. Albertini, M. Solzi, Tuning the magnetic and magnetocaloric properties of austenitic Ni-Mn-(In,Sn)Heuslers, Scr. Mater. (2019). https://doi.org/10.1016/j.scriptamat.2019.05.027.

[15] T. Krenke, E. Duman, M. Acet, E.F. Wassermann, X. Moya, L. Mañosa, A. Planes, E. Suard, B. Ouladdiaf, Magnetic superelasticity and inverse magnetocaloric effect in Ni-Mn-In, Phys. Rev. B - Condens. Matter Mater. Phys. 75 (2007). https://doi.org/10.1103/PhysRevB.75.104414.

[16] L. Pareti, M. Solzi, F. Albertini, A. Paoluzi, Giant entropy change at the co-occurrence of structural and magnetic transitions in the Ni2.19Mn0.81Ga Heusler alloy, Eur. Phys. J. B. 32 (2003) 303–307. https://doi.org/10.1140/epjb/e2003-00102-y.

[17] P. Entel, M. Siewert, M.E. Gruner, H.C. Herper, D. Comtesse, R. Arróyave, N. Singh, A. Talapatra, V. V. Sokolovskiy, V.D. Buchelnikov, F. Albertini, L. Righi, V.A. Chernenko, Complex magnetic ordering as a driving mechanism of multifunctional properties of Heusler alloys from first principles, Eur. Phys. J. B. (2013). https://doi.org/10.1140/epjb/e2012-30936-9.

[18] V.D. Buchelnikov, P. Entel, S. V. Taskaev, V. V. Sokolovskiy, A. Hucht, M. Ogura, H. Akai, M.E. Gruner, S.K. Nayak, Monte Carlo study of the influence of antiferromagnetic exchange interactions on the phase transitions of ferromagnetic Ni-Mn-X alloys (X=In,Sn,Sb), Phys. Rev. B - Condens. Matter Mater. Phys. (2008). https://doi.org/10.1103/PhysRevB.78.184427.

[19] E. Şaşioğlu, L.M. Sandratskii, P. Bruno, Role of conduction electrons in mediating exchange interactions in Mn-based Heusler alloys, Phys. Rev. B - Condens. Matter Mater. Phys. (2008). https://doi.org/10.1103/PhysRevB.77.064417.

[20] V.D. Buchelnikov, V. V. Sokolovskiy, Magnetocaloric effect in Ni-Mn-X (X = Ga, In, Sn, Sb) heusler alloys, Phys. Met. Metallogr. (2011). https://doi.org/10.1134/S0031918X11070052.

[21] Z.D. Han, D.H. Wang, C.L. Zhang, H.C. Xuan, J.R. Zhang, B.X. Gu, Y.W. Du, Effect of lattice contraction on martensitic transformation and magnetocaloric effect in Ge doped Ni-Mn-Sn alloys, Mater. Sci. Eng. B Solid-State Mater. Adv. Technol. 157 (2009). https://doi.org/10.1016/j.mseb.2008.12.006.

[22] L. Mañosa, X. Moya, A. Planes, O. Gutfleisch, J. Lyubina, M. Barrio, J.L. Tamarit, S. Aksoy, T. Krenke, M. Acet, Effects of hydrostatic pressure on the magnetism and martensitic transition of Ni-Mn-In magnetic superelastic alloys, Appl. Phys. Lett. (2008). https://doi.org/10.1063/1.2830999.

[23] D.N. Lobo, K.R. Priolkar, P.A. Bhobe, D. Krishnamurthy, S. Emura, Correlation between local structure distortions and martensitic transformation in Ni-Mn-In alloys, Appl. Phys. Lett. (2010). https://doi.org/10.1063/1.3454277.

[24] R. Nevgi, G. Das, M. Acet, K.R. Priolkar, Importance of site occupancy and absence of strain glassy phase in Ni2−xFexMn1.5In0.5, J. Alloys Compd. 797 (2019). https://doi.org/10.1016/j.jallcom.2019.05.172.

[25] K.R. Priolkar, P.A. Bhobe, D.N. Lobo, S.W. D'Souza, S.R. Barman, A. Chakrabarti, S. Emura, Antiferromagnetic exchange interactions in the Ni2Mn 1.4In0.6 ferromagnetic Heusler alloy, Phys. Rev. B - Condens. Matter Mater. Phys. (2013). https://doi.org/10.1103/PhysRevB.87.144412.

[26] V. V. Sokolovskiy, V.D. Buchelnikov, M.A. Zagrebin, A. Grünebohm, P. Entel, Predictions of a Large Magnetocaloric Effect in Co- and Cr-Substituted Heusler Alloys Using First-Principles and Monte Carlo Approaches, in: Phys. Procedia, 2015. https://doi.org/10.1016/j.phpro.2015.12.155.

[27] V. V. Sokolovskiy, V.D. Buchelnikov, S. V. Taskaev, V. V. Khovaylo, M. Ogura, P. Entel, Quaternary Ni-Mn-In-Y Heusler alloys: A way to achieve materials with better magnetocaloric properties?, J. Phys. D. Appl. Phys. (2013). https://doi.org/10.1088/0022-3727/46/30/305003.

[28] A. Taubel, B. Beckmann, L. Pfeuffer, N. Fortunato, F. Scheibel, S. Ener, T. Gottschall, K.P. Skokov, H. Zhang, O. Gutfleisch, Tailoring magnetocaloric effect in all-d-metal Ni-Co-Mn-Ti Heusler alloys: a combined experimental and theoretical study, Acta Mater. 201 (2020). https://doi.org/10.1016/j.actamat.2020.10.013.

[29] S.W. D'Souza, A. Chakrabarti, S.R. Barman, Magnetic interactions and electronic structure of Ni-Mn-In, J. Electron Spectros. Relat. Phenomena. 208 (2016) 33–39. https://doi.org/10.1016/j.elspec.2015.10.003.

[30] J. Lyubina, Magnetocaloric materials for energy efficient cooling, J. Phys. D. Appl. Phys. (2017). https://doi.org/10.1088/1361-6463/50/5/053002.

[31] P. Entel, M.E. Gruner, S. Fähler, M. Acet, A. Çahır, R. Arróyave, S. Sahoo, T.C. Duong, A. Talapatra, L. Sandratskii, S. Mankowsky, T. Gottschall, O. Gutfleisch, P. Lázpita, V.A. Chernenko, J.M. Barandiaran, V. V. Sokolovskiy, V.D. Buchelnikov, Probing Structural and Magnetic Instabilities and Hysteresis in Heuslers by Density Functional Theory Calculations, Phys. Status Solidi Basic Res. (2018). https://doi.org/10.1002/pssb.201700296.

[32] O. Gutfleisch, T. Gottschall, M. Fries, D. Benke, I. Radulov, K.P. Skokov, H. Wende, M. Gruner, M. Acet, P. Entel, M. Farle, Mastering hysteresis in magnetocaloric materials, Philos. Trans. R. Soc. A Math. Phys. Eng. Sci. 374 (2016). https://doi.org/10.1098/rsta.2015.0308.

[33] I. Titov, M. Acet, M. Farle, D. González-Alonso, L. Mañosa, A. Planes, T. Krenke, Hysteresis effects in the inverse magnetocaloric effect in martensitic Ni-Mn-In and Ni-Mn-Sn, J. Appl. Phys. (2012). https://doi.org/10.1063/1.4757425.

[34] V. Sokolovskiy, M. Zagrebin, V. Buchelnikov, P. Entel, Monte Carlo Simulations of Thermal Hysteresis in Ni-Mn-Based Heusler Alloys, Phys. Status Solidi Basic Res. 255 (2018). https://doi.org/10.1002/pssb.201700265.

[35] V. Basso, C.P. Sasso, K.P. Skokov, O. Gutfleisch, V. V. Khovaylo, Hysteresis and magnetocaloric effect at the magnetostructural phase transition of Ni-Mn-Ga and Ni-Mn-Co-Sn Heusler alloys, Phys. Rev. B - Condens. Matter Mater. Phys. 85 (2012) 1–8. https://doi.org/10.1103/PhysRevB.85.014430.

[36] T. Gottschall, K. Skokov, M. Fries, A. Taubel, I. Radulov, F. Scheibel, D. Benke, S. Riegg, O. Gutfleisch, Making a Cool Choice: The Materials Library of Magnetic Refrigeration, Adv. En. Mater. 9 (2019) 1901322. https://doi.org/10.1002/aenm.201901322.

[37] S. Singh, L. Caron, S.W. D'Souza, T. Fichtner, G. Porcari, S. Fabbrici, C. Shekhar, S. Chadov, M. Solzi, C. Felser, Large Magnetization and Reversible Magnetocaloric Effect at the Second-Order Magnetic Transition in Heusler Materials, Adv. Mater. (2016). https://doi.org/10.1002/adma.201505571.

[38] S. Ghosh, S. Ghosh, Cosubstitution in Ni-Mn-Sb Heusler compounds: Realization of room-temperature reversible magnetocaloric effect driven by second-order magnetic transition, Phys. Rev. Mater. 4 (2020). https://doi.org/10.1103/PhysRevMaterials.4.025401.

[39] Y. Feng, J.H. Sui, Z.Y. Gao, J. Zhang, W. Cai, Investigation on martensitic transformation behavior, microstructures and mechanical properties of Fe-doped Ni-Mn-In alloys, Mater. Sci. Eng. A. 507 (2009). https://doi.org/10.1016/j.msea.2008.12.003.

[40] R. Nevgi, K.R. Priolkar, Unusual strain glassy phase in Fe doped Ni2Mn1.5In0.5, Appl. Phys. Lett. 112 (2018). https://doi.org/10.1063/1.5004054.

[41] M. Youcef, A. Bouhalouane, D.K. Kouider, A. Hamza, Magneto-electronic and Thermodynamic Properties of Quaternary NiFeMnZ (Z = In, Sn) New Spin Gapless Semiconductors, J. Supercond. Nov. Magn. 32 (2019). https://doi.org/10.1007/s10948-018-4687-7.

[42] V.K. Sharma, M.K. Chattopadhyay, S.K. Nath, K.J.S. Sokhey, R. Kumar, P. Tiwari, S.B. Roy, The effect of substitution of Mn by Fe and Cr on the martensitic transition in the Ni50Mn34In16 alloy, J. Phys. Condens. Matter. 22 (2010). https://doi.org/10.1088/0953-8984/22/48/486007.

[43] V.K. Sharma, M.K. Chattopadhyay, A. Khandelwal, S.B. Roy, Martensitic transition near room temperature and the temperature- and magnetic-field-induced multifunctional properties of Ni49 CuMn 34 In16 alloy, Phys. Rev. B - Condens. Matter Mater. Phys. 82 (2010) 1–4. https://doi.org/10.1103/PhysRevB.82.172411.

[44] M.K. Chattopadhyay, V.K. Sharma, A. Chouhan, P. Arora, S.B. Roy, Combined effect of hydrostatic pressure and magnetic field on the martensitic transition in the Ni49CuMn34In16 alloy, Phys. Rev. B - Condens. Matter Mater. Phys. 84 (2011) 1–9. https://doi.org/10.1103/PhysRevB.84.064417.

[45] J. Liu, X. Fei, Y. Gong, F. Xu, Phase transition and magnetocaloric properties of Ni50Mn35-xIn15Cux bulk alloys and ribbons, IEEE Trans. Magn. 51 (2015). https://doi.org/10.1109/TMAG.2015.2441377.

[46] Y. Ma, H. Hao, Y. Xin, H. Luo, H. Liu, F. Meng, E. Liu, Atomic ordering and magnetic properties of quaternary Heusler alloys NiCuMnZ (Z=In, Sn, Sb), Intermetallics. 86 (2017). https://doi.org/10.1016/j.intermet.2017.03.020.

[47] G. Porcari, M. Buzzi, F. Cugini, R. Pellicelli, C. Pernechele, L. Caron, E. Brück, M. Solzi, Direct magnetocaloric characterization and simulation of thermomagnetic cycles, Rev. Sci. Instrum. 84 (2013). https://doi.org/10.1063/1.4815825.

[48] L.C. Chapon, P. Manuel, P.G. Radaelli, C. Benson, L. Perrott, S. Ansell, N.J. Rhodes, D. Raspino, D. Duxbury, E. Spill, J. Norris, Wish: The new powder and single crystal magnetic diffractometer on the second target station, Neutron News. 22 (2011). https://doi.org/10.1080/10448632.2011.569650.

[49] V. Petrícek, M. Dušek, L. Palatinus, Crystallographic computing system JANA2006: General features, Zeitschrift Fur Krist. (2014). https://doi.org/10.1515/zkri-2014-1737.

[50] T. Miyamoto, W. Ito, R.Y. Umetsu, R. Kainuma, T. Kanomata, K. Ishida, Phase stability and magnetic properties of Ni50Mn50-xInx Heusler-type alloys, Scr. Mater. (2010). https://doi.org/10.1016/j.scriptamat.2009.10.006.

[51] C. Bennati, S. Fabbrici, R. Cabassi, N.S. AMADè, F. Cugini, M. Solzi, F. Albertini, Curie temperature effect on the inverse MCE in Ni2MnIn based Heusler alloys near room temperature, in: Refrig. Sci. Technol., International Institute of Refrigeration, 2018: pp. 262–267. https://doi.org/10.18462/iir.thermag.2018.0043.

[52] T. Krenke, M. Acet, E.F. Wassermann, X. Moya, L. Mañosa, A. Planes, Ferromagnetism in the austenitic and martensitic states of Ni-Mn-In alloys, Phys. Rev. B - Condens. Matter Mater. Phys. 73 (2006). https://doi.org/10.1103/PhysRevB.73.174413.

[53] V. Recarte, J.I. Pérez-Landazábal, V. Sánchez-Alarcos, J.A. Rodríguez-Velamazán, Dependence of the martensitic transformation and magnetic transition on the atomic order in Ni-Mn-In metamagnetic shape memory alloys, Acta Mater. (2012). https://doi.org/10.1016/j.actamat.2012.01.020.

[54] N. Yamada, Atomic Magnetic Moment and Exchange Interaction between Mn Atoms in Intermetallic Compounds in Mn-Ge System [J. Phys. Soc. Jpn. 59 (1990) 273], J. Phys. Soc. Japan. 59 (1990). https://doi.org/10.1143/JPSJ.59.4199.

[55] A. Çaklr, M. Acet, M. Farle, Shell-ferromagnetism of nano-Heuslers generated by segregation under magnetic field, Sci. Rep. 6 (2016). https://doi.org/10.1038/srep28931.

[56] Z. Wu, Z. Liu, H. Yang, Y. Liu, G. Wu, R.C. Woodward, Metallurgical origin of the effect of Fe doping on the martensitic and magnetic transformation behaviours of Ni50Mn40-xSn 10Fex magnetic shape memory alloys, Intermetallics. 19 (2011). https://doi.org/10.1016/j.intermet.2010.10.010.

[57] E.C. Passamani, F. Xavier, E. Favre-Nicolin, C. Larica, A.Y. Takeuchi, I.L. Castro, J.R. Proveti, Magnetic properties of NiMn-based Heusler alloys influenced by Fe atoms replacing Mn, J. Appl. Phys. 105 (2009). https://doi.org/10.1063/1.3075835.

[58] F. Orlandi, A. Çaklr, P. Manuel, D.D. Khalyavin, M. Acet, L. Righi, Neutron diffraction and symmetry analysis of the martensitic transformation in Co-doped Ni2MnGa, Phys. Rev. B. 101 (2020). https://doi.org/10.1103/PhysRevB.101.094105.

[59] T. Graf, C. Felser, S.S.P. Parkin, Simple rules for the understanding of Heusler compounds, Prog. Solid State Chem. (2011). https://doi.org/10.1016/j.progsolidstchem.2011.02.001.

[60] F. Orlandi, S. Fabbrici, F. Albertini, P. Manuel, D.D. Khalyavin, L. Righi, Long-range antiferromagnetic interactions in Ni-Co-Mn-Ga metamagnetic Heusler alloys: A two-step ordering studied by neutron diffraction, Phys. Rev. B. (2016). https://doi.org/10.1103/PhysRevB.94.140409.

[61] F. Cugini, M. Solzi, On the direct measurement of the adiabatic temperature change of magnetocaloric materials, J. Appl. Phys. (2020). https://doi.org/10.1063/5.0002870.

[62] A.M. Tishin, Y.I. Spichkin, Magnetocloric Effect and Its Applications.pdf, Ser. Condens. Matter Phys. (2003) 4–401.

[63] V. V. Sokolovskiy, M.E. Gruner, P. Entel, M. Acet, A. Cakir, D.R. Baigutlin, V.D. Buchelnikov, Segregation tendency of Heusler alloys, Phys. Rev. Mat. 3 (2019).

[64] L. Chen, F.X. Hu, J. Wang, J. Shen, J.R. Sun, B.G. Shen, J.H. Yin, L.Q. Pan, Q.Z. Huang, Effect of post-annealing on martensitic transformation and magnetocaloric effect in Ni45Co5Mn36.7In13.3 alloys, in: J. Appl. Phys., 2011. https://doi.org/10.1063/1.3565189.

[65] W. Ito, M. Nagasako, R.Y. Umetsu, R. Kainuma, T. Kanomata, K. Ishida, Atomic ordering and magnetic properties in the Ni45Co 5Mn36.7In13.3 metamagnetic shape memory alloy, Appl. Phys. Lett. (2008). https://doi.org/10.1063/1.3043456.

[66] N.M. Bruno, D. Salas, S. Wang, I. V. Roshchin, R. Santamarta, R. Arroyave, T. Duong, Y.I. Chumlyakov, I. Karaman, On the microstructural origins of martensitic transformation arrest in a NiCoMnIn magnetic shape memory alloy, Acta Mater. (2018). https://doi.org/10.1016/j.actamat.2017.08.037.

[67] J. Liang, M. Masche, K. Engelbrecht, K. Nielsen, H. Vieyra, A. Barcza, C. Bahl, Experimental study of non-bonded packed bed active magnetic regenerators with stabilized La(Fe,Mn,Si)$_{13}$H$_y$ particles, Appl. Therm. Eng. 197 (2021) 117383. https://doi.org/10.1016/j.applthermaleng.2021.117383

Table I: Table of the EDX elemental analysis of Mn(Ni) series as a function of the increasing x for the nominal compositions $Ni_{50-x}Mn_{34+x}In_{16}$. (*) The Curie temperature evaluated from Arrot plots built on magnetization data.

| label | Nominal comp. (at.%) | Measured comp. (at.%) ±0.2% | $T_C$ (K) ±1.5 K | $T_M$ (K) ±1.5 K | $M_S$ @ 80 K ($Am^2/Kg$) ± 1.2 $Am^2/Kg$ |
|---|---|---|---|---|---|
| x=-2 | $Ni_{52}Mn_{32}In_{16}$ | $Ni_{52.3}Mn_{31.1}In_{18.1}$ | 298 * | 310.8 | – |
| x=0 | $Ni_{50}Mn_{34}In_{16}$ | $Ni_{49.7}Mn_{34.2}In_{16.2}$ | 312.1 | 300.7 | – |
| x=1 | $Ni_{49}Mn_{35}In_{16}$ | $Ni_{49}Mn_{32.9}In_{18.1}$ | 316.5 | – | 127.1 |
| x=2 | $Ni_{48}Mn_{36}In_{16}$ | $Ni_{48.1}Mn_{34.7}In_{17.2}$ | 315.8 | – | 125.7 |
| x=3 | $Ni_{47}Mn_{37}In_{16}$ | $Ni_{47.4}Mn_{35.1}In_{17.5}$ | 316.2 | – | 124.9 |
| x=6 | $Ni_{44}Mn_{40}In_{16}$ | $Ni_{43.9}Mn_{39.4}In_{16.7}$ | 317.4 | – | 122.7 |

Table II: Table of the EDX elemental analysis of the main phases of Cu(Mn) and Fe(Mn) series. (*) The low temperature $M_S$ value has been extrapolated due to the presence of martensitic transition by fitting the magnetization curve with a Brillouin function. (**) The values refer to samples additionally heat treated at 1173 K.

| label | Nominal comp. (at.%) | Measured comp. (at.%) ±0.2% | $T_C$ (K) ±1.5 K | $T_M$ (K) ±1.5 K | $M_S$ @ 80 K ($Am^2/Kg$) ± 1.2 $Am^2/Kg$ |
|---|---|---|---|---|---|
| Cu,Fe0 (x=2) | $Ni_{48}Mn_{36}In_{16}$ | $Ni_{48.1}Mn_{34.7}In_{17.2}$ | 314.9 | – | 125.7 |
| Cu4 | $Ni_{48}Mn_{32}\mathbf{Cu_4}In_{16}$ | $Ni_{47.8}Mn_{31.2}\mathbf{Cu_{3.8}}In_{17.1}$ | 297.4 | – | 117 |
| Cu5 | $Ni_{48}Mn_{31}\mathbf{Cu_5}In_{16}$ | $Ni_{47.9}Mn_{29.9}\mathbf{Cu_5}In_{17.1}$ | 293.3 | – | 108 |
| Cu6 | $Ni_{48}Mn_{30}\mathbf{Cu_6}In_{16}$ | $Ni_{48.1}Mn_{28.4}\mathbf{Cu_{5.9}}In_{17.5}$ | 281.1 | 223 | 88* |
| Cu8 | $Ni_{48}Mn_{28}\mathbf{Cu_8}In_{16}$ | $Ni_{44.6}Mn_{26.9}\mathbf{Cu_{9.6}}In_{18.9}$ (main)<br>$Ni_{52.6}Mn_{27.7}\mathbf{Cu_{15.9}}In_{3.8}$ (inclusions) | 288.7 (main) | – | – |
| Cu8** | $Ni_{48}Mn_{28}\mathbf{Cu_8}In_{16}$ | $Ni_{48.6}Mn_{27.5}\mathbf{Cu_{7.6}}In_{16.2}$ | 271.4 | 227 | 85* |
| Fe2 | $Ni_{48}Mn_{34}\mathbf{Fe_2}In_{16}$ | $Ni_{47.6}Mn_{32.2}\mathbf{Fe_{2.4}}In_{17.8}$ | 319.2 | – | 131 |
| Fe4 | $Ni_{48}Mn_{32}\mathbf{Fe_4}In_{16}$ | $Ni_{48.8}Mn_{30.4}\mathbf{Fe_{3.7}}In_{17}$ | 323.4 | – | 133 |
| Fe5 | $Ni_{48}Mn_{31}\mathbf{Fe_5}In_{16}$ | $Ni_{48.4}Mn_{29.6}\mathbf{Fe_{4.7}}In_{17.3}$ | 325 | – | 121.6 |
| Fe10 | $Ni_{48}Mn_{26}\mathbf{Fe_{10}}In_{16}$ | $Ni_{49.9}Mn_{27.1}\mathbf{Fe_{4.1}}In_{18.9}$ (main)<br>Fe (inclusions) | 329/344 | – | – |
| Fe10** | $Ni_{48}Mn_{26}\mathbf{Fe_{10}}In_{16}$ | $Ni_{48.2}Mn_{27.8}\mathbf{Fe_{5.8}}In_{18.5}$ | 337.9 | – | 110 |

Table III: EDX elemental analysis of Fe-Cu(Mn) series, annealed at 1073 K for 72 h or at 1173 K for 24 h. (*) The low temperature $M_S$ value has been extrapolated due to the presence of martensitic transition by fitting the magnetization curve with a Brillouin function.

| label | Nominal comp. (at.%) | Measured comp. (at.%) ±0.2% | $T_C$ (K) ±1.5 K | $T_M$ (K) ±1.5 K | $M_S$ @ 80 K ($Am^2/Kg$) ±1 $Am^2/Kg$ | $\Delta T_{ad}^{max}$ (K) ±0.07 K |
|---|---|---|---|---|---|---|
| | annealing 1073 K | | | | | |
| Cu5.4Fe0.6 | $Ni_{48}Mn_{30}\mathbf{Fe_{0.6}Cu_{5.4}}In_{16}$ | $Ni_{46.7}Mn_{31.9}\mathbf{Fe_{0.3}Cu_{5.3}}In_{15.8}$ | 290 | 233 | 103* | 0.64 |
| Cu5.7Fe1.3 | $Ni_{48}Mn_{29}\mathbf{Fe_{1.3}Cu_{5.7}}In_{16}$ | $Ni_{46.2}Mn_{30.9}\mathbf{Fe_{0.7}Cu_{5.8}}In_{16.5}$ | 293 | – | 113 | 0.82 |
| Cu6Fe2 | $Ni_{48}Mn_{28}\mathbf{Fe_2Cu_6}In_{16}$ | $Ni_{47.6}Mn_{28.6}\mathbf{Fe_{1.6}Cu_{6.2}}In_{16}$ | 299 | – | 106 | 0.78 |
| | Annealing 1173 K | | | | | |

| | | | | | | |
|---|---|---|---|---|---|---|
| Cu6.4Fe0.6 | $Ni_{48}Mn_{29}\mathbf{Fe_{0.6}Cu_{6.4}}In_{16}$ | $Ni_{45.6}Mn_{32.4}\mathbf{Fe_{0.4}Cu_{5.3}}In_{16.3}$ | 290 | 198 | 110* | 0.74 |
| Cu6.4Fe2.6 | $Ni_{48}Mn_{27}\mathbf{Fe_{2.6}Cu_{6.4}}In_{16}$ | $Ni_{47.1}Mn_{27.9}\mathbf{Fe_{2.5}Cu_{6.4}}In_{16}$ | 295 | – | 98 | 0.74 |
| Cu6.8Fe3.2 | $Ni_{48}Mn_{26}\mathbf{Fe_{3.2}Cu_{6.8}}In_{16}$ | $Ni_{46.7}Mn_{26.8}\mathbf{Fe_{2.9}Cu_{6.8}}In_{16.8}$ | 297 | – | 91 | 0.58 |

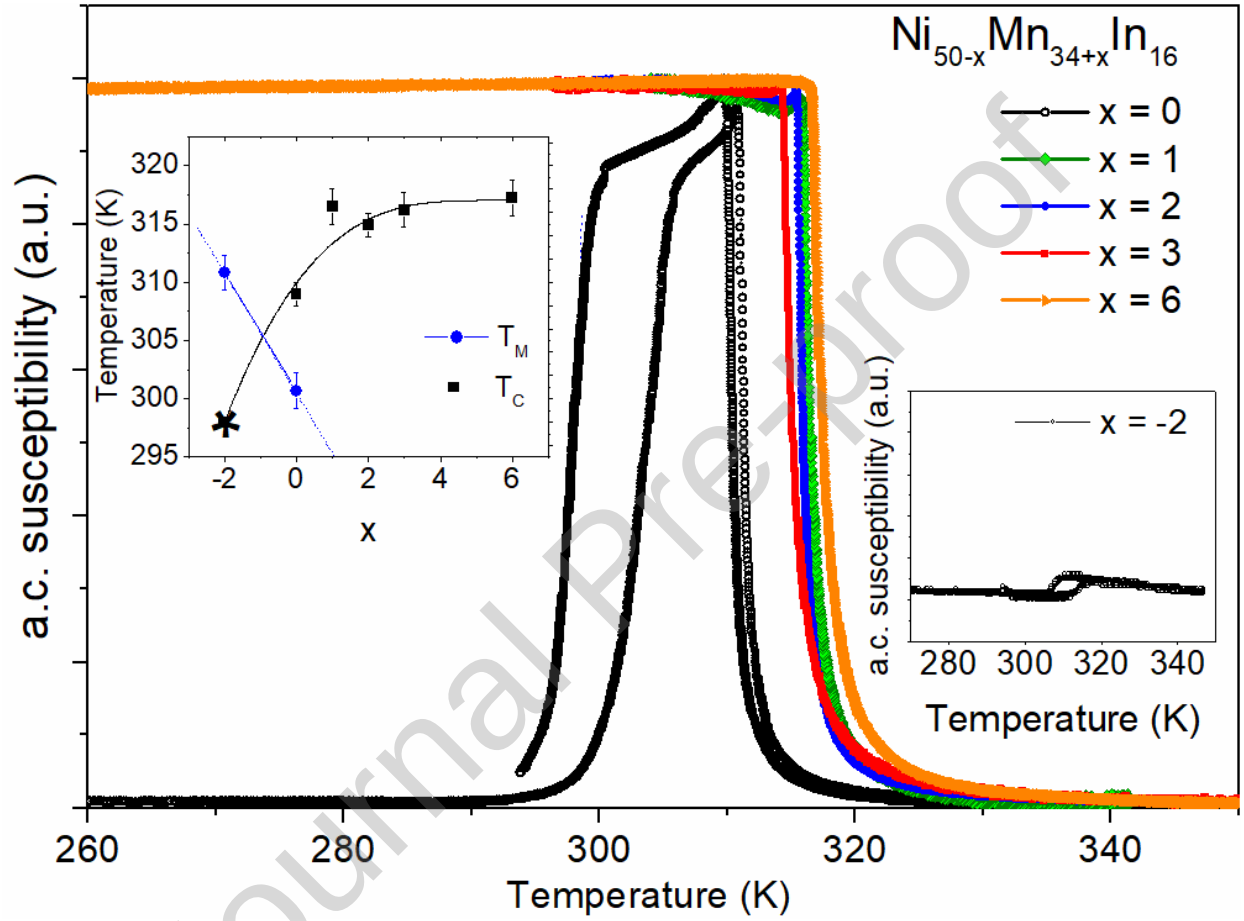


Figure 1: Low magnetic field thermo magnetic analysis (a.c. susceptibility as a function of temperature) of r the ternary $Ni_{50-x}Mn_{36+x}In_{16}$ compounds of Table I. The left inset shows a portion of the magneto structural phase diagram for these samples as a function of Mn; the lines are guides to the eye. The Curie temperature marked with the * symbol is computed from Arrot Plots. The right inset is a magnification of the susceptibility signal for sample x= -2, where the martensitic transformation occurs above the austenitic Curie temperature.

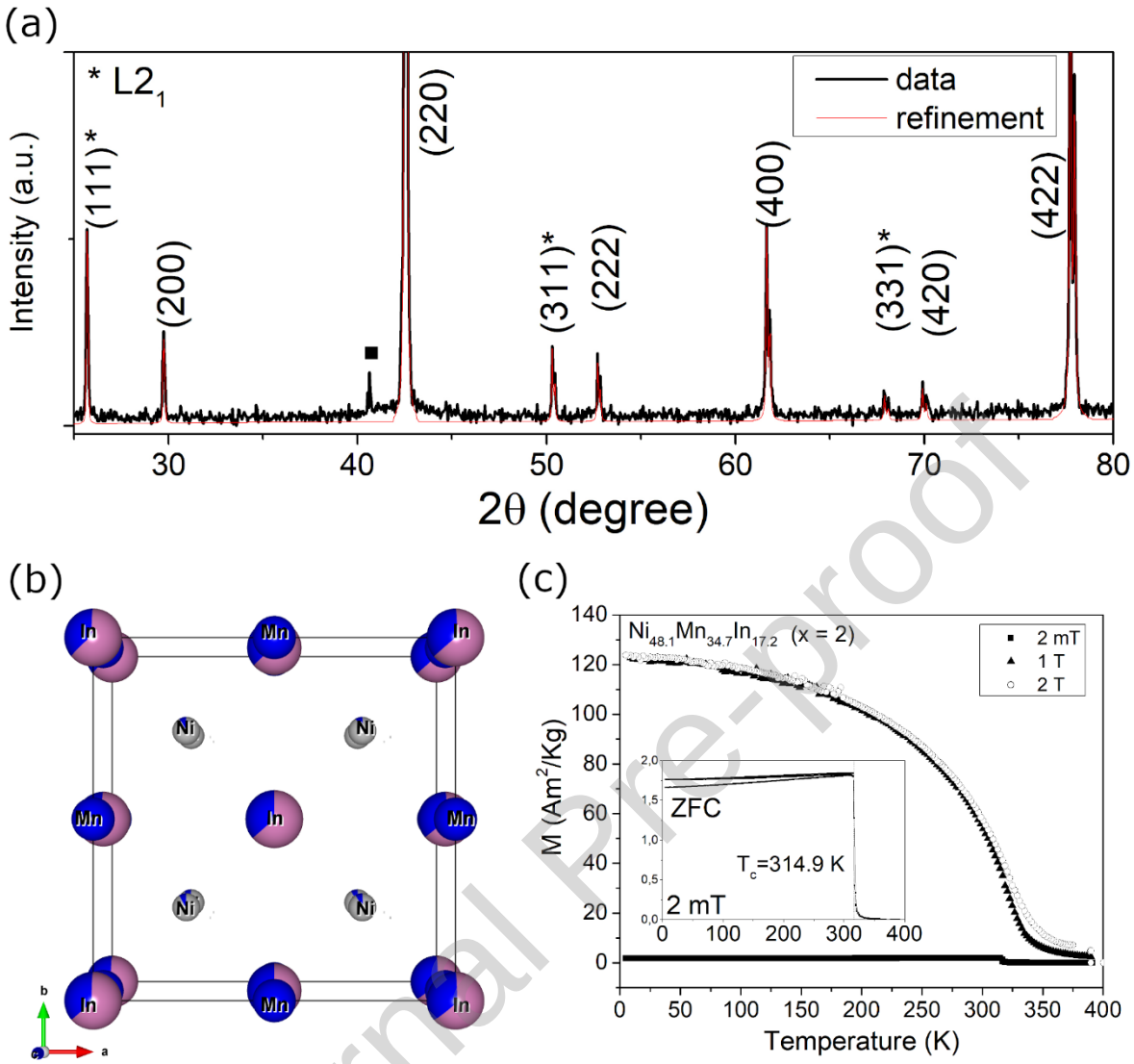


Figure 2: (a) X-ray diffraction pattern at room temperature of the $Ni_{48}Mn_{36}In_{16}$ (x=2) sample. The * marks the $L2_1$ superstructure reflections. The red line is the LeBail peak fitting. The square symbol marks a reflection from the sample holder. (b) Cubic cell and expected occupancy (drawing produced with VESTA [29]) and (c) Iso-field ($\mu_0$H=2mT, 1T, 2T) magnetization curves as a function of temperature.

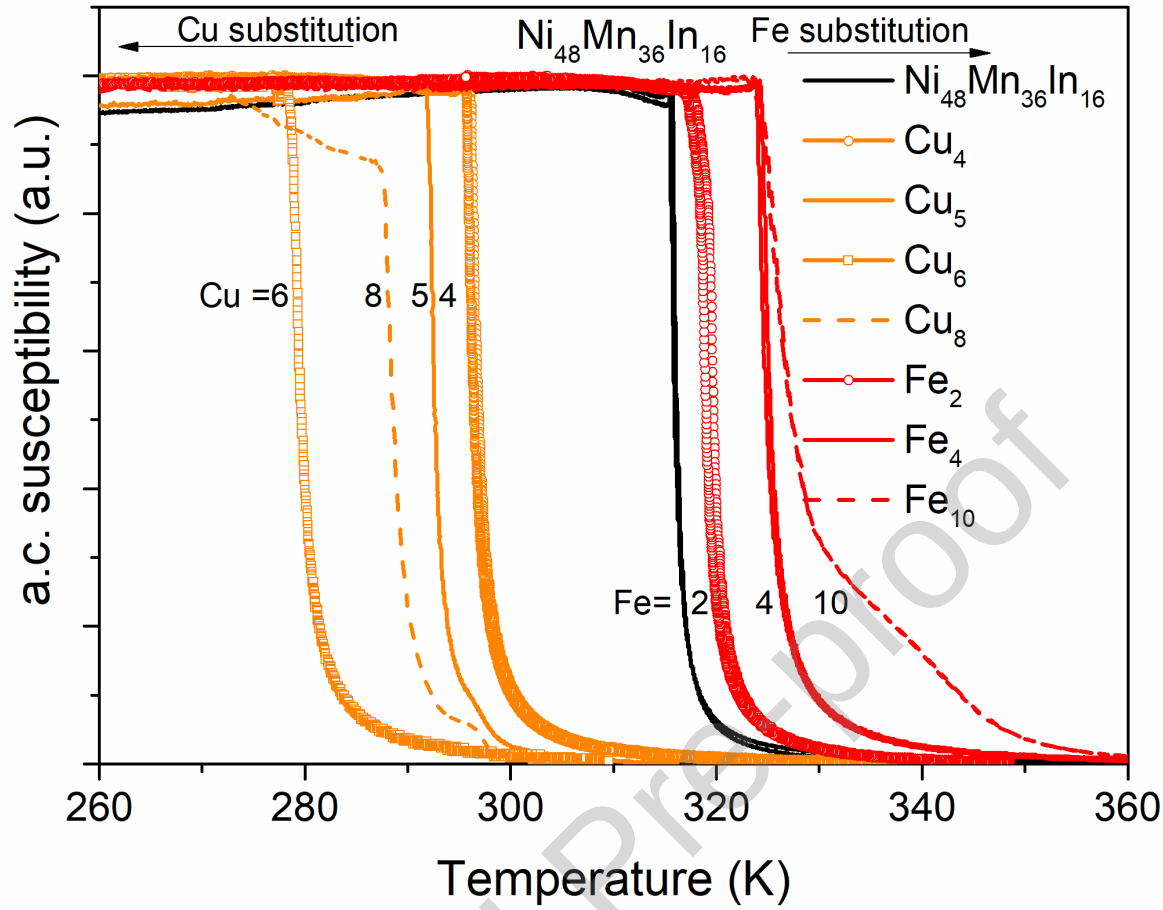


Figure 3: Thermo magnetic analysis (a.c. susceptibility as a function of temperature) for the Cu(Mn) and Fe(Mn) series.

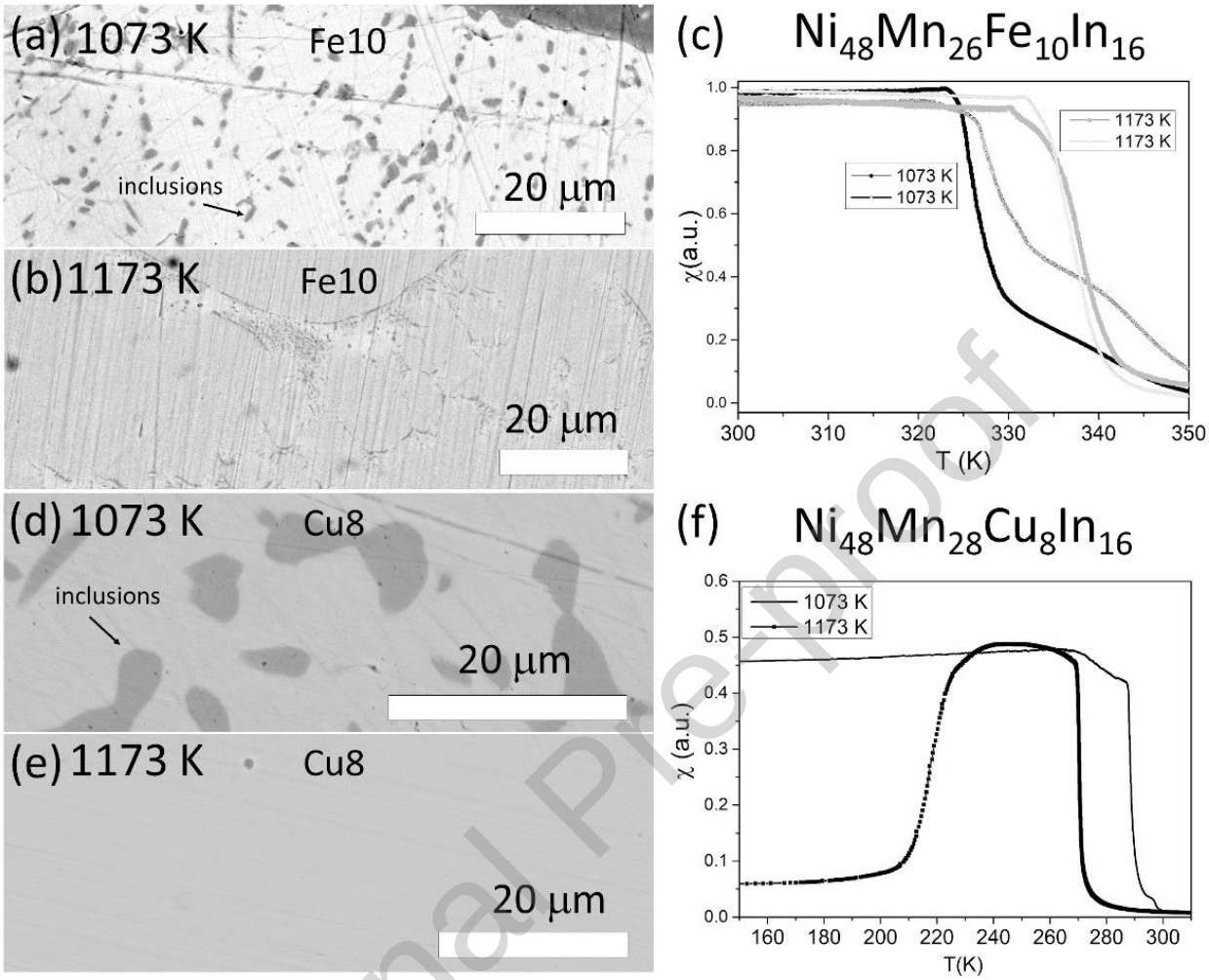


Figure 4: (a) and (b) SEM-BS images of sample Fe10 and (d) and (e) of sample Cu8 of Table II before (a,d) and after (b,e) the second annealing at 1173 K. (c) and (f) comparison of the a.c. susceptibility of the two samples before and after the secondary heat treatment at 1173 K. Note that in sample Fe10 two fragments with different thermomagnetic response show a very similar susceptibility profile after the secondary heat treatment.

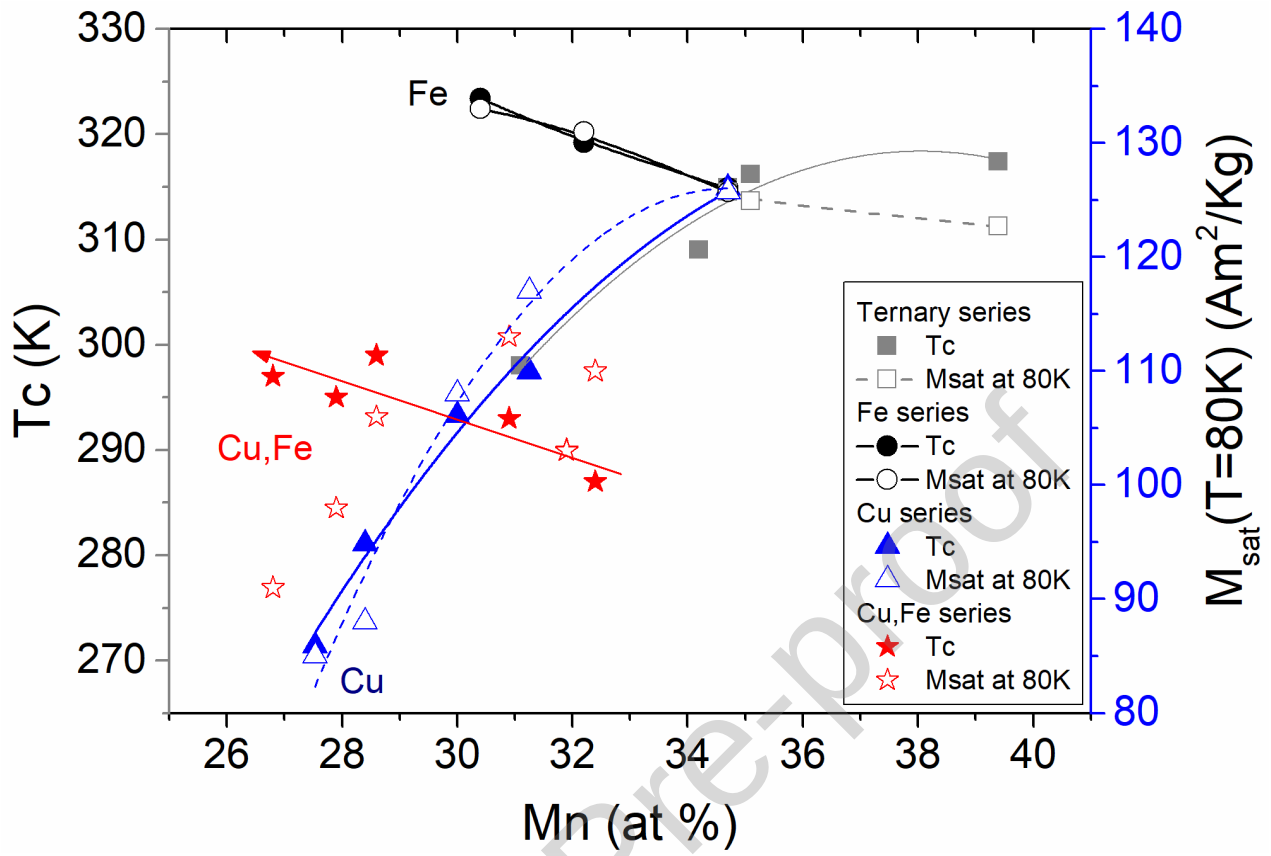


Figure 5: Curie temperature (left axis, solid symbols) and saturation magnetization (right axis, hollow symbols) values as a function of the Mn content for the four series. The error bars are comprised within the size of the symbols used. The lines (solid, $T_C$ curves; dashed, $M_{sat}$ curves) are guides to the eye

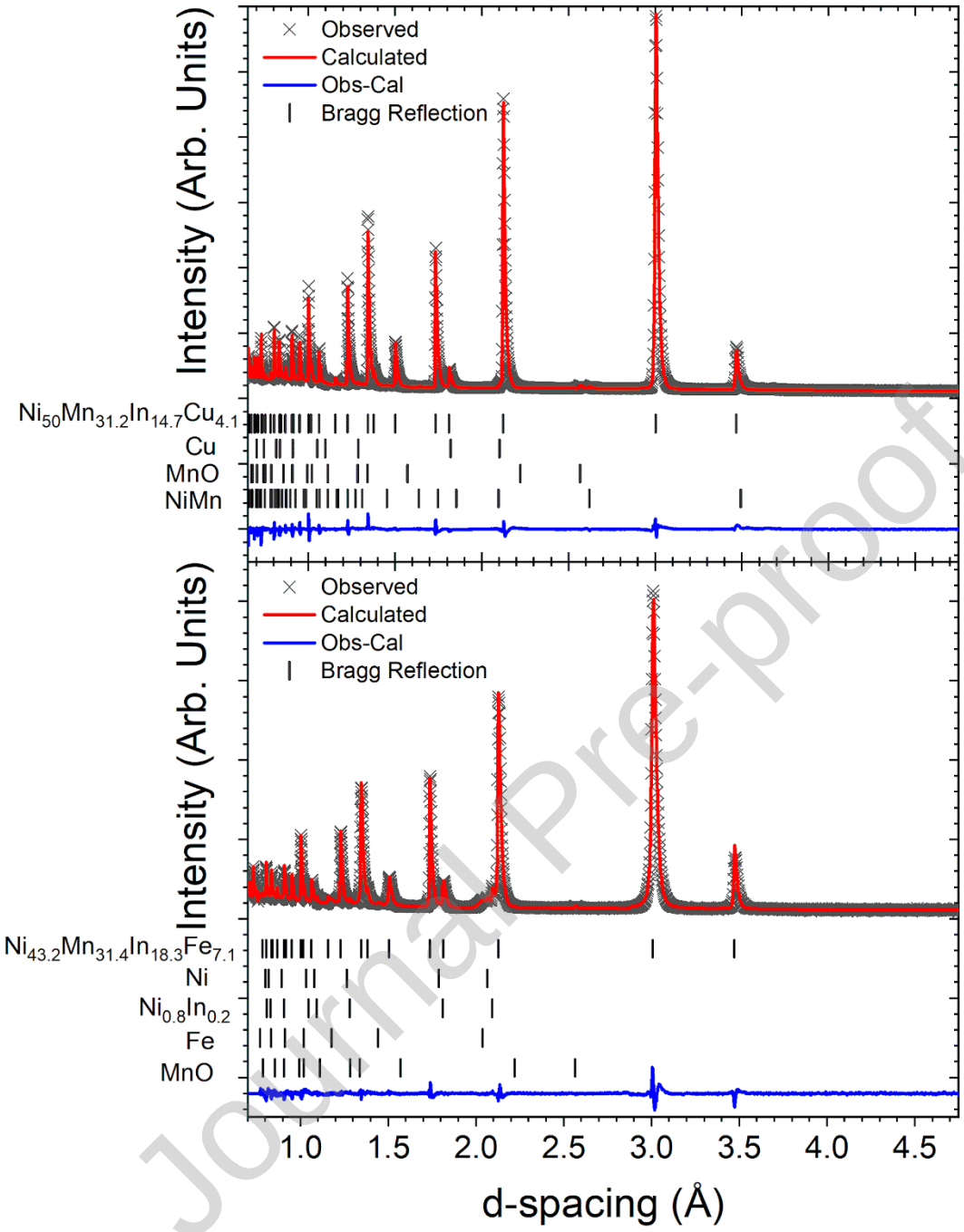


Figure 6: Rietveld plot of the $Ni_{48}Mn_{31}Cu_5In_{16}$ (top) at 350 K and $Ni_{48}Mn_{31}Fe_5In_{16}$ (bottom) at 360 K, collected on the WISH diffractometer on the detector bank with average 2-θ of 121.6 degrees. Observed (x-black), Calculated (red-line), difference (blue-line) are reported. The tick marks represent the Bragg positions of the main and impurity phases. The refined atomic composition for the main phases are $Ni_{52.6}Mn_{27.7}In_{3.8}Cu_{15.9}$ and $Ni_{43(2)}Mn_{31.46(6)}In_{18.25(3)}Fe_{7(2)}$. The overall reliability factors are Rp=3.87% wRp=4.70% for $Ni_{48}Mn_{31}Cu_5In_{16}$ and Rp=4.23% wRp=4.65% for $Ni_{48}Mn_{31}Fe_5In_{16}$.

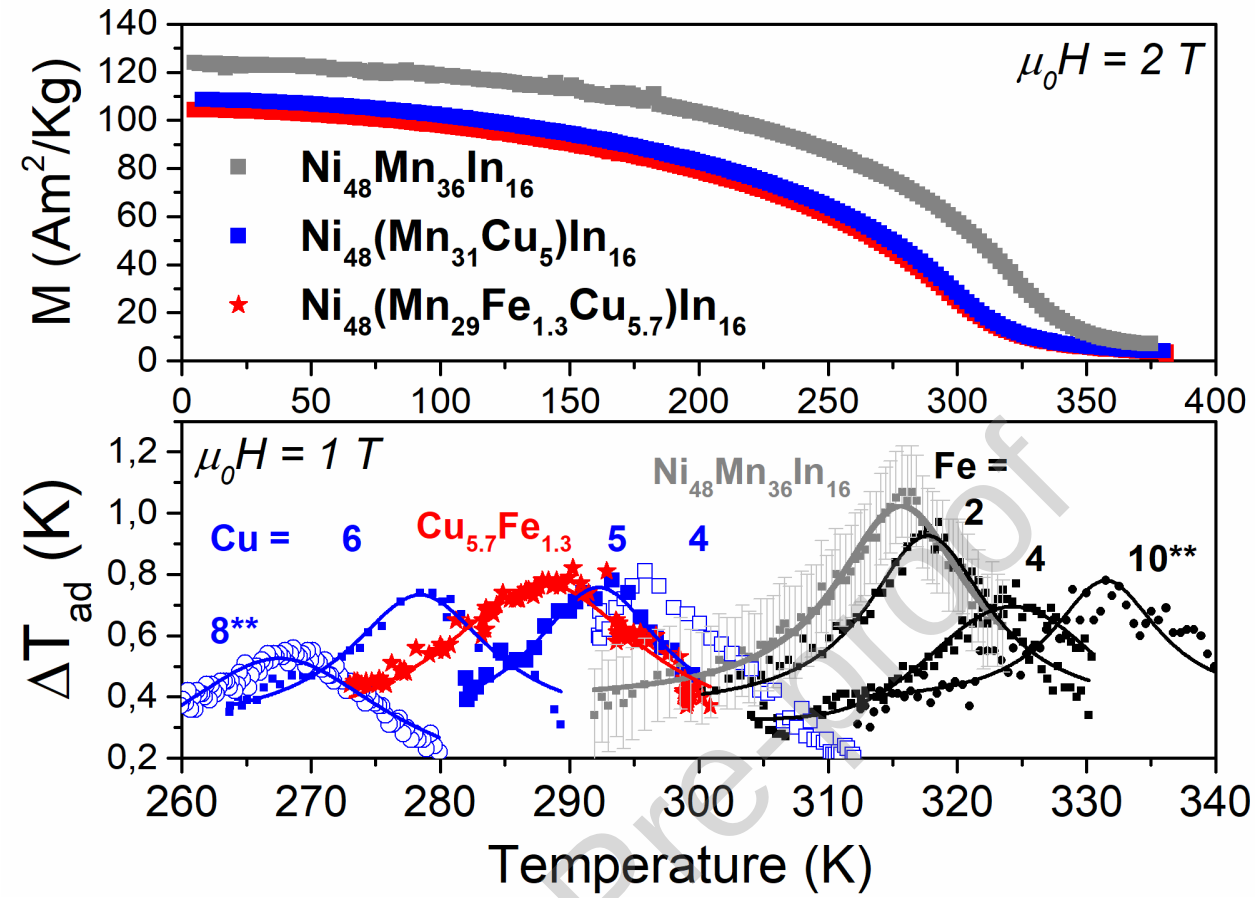


Figure 7: Top panel: Iso-field ($\mu_0$H=2T) magnetization curves as a function of temperature of selected samples compared to the ternary $Ni_{48}Mn_{36}In_{16}$ (x=2) sample. Bottom panel: adiabatic temperature change $\Delta T_{ad}$ in samples homogenized at 1073 K for the four series: the labels close to the various curves highlight the nominal composition of the doping elements as defined in Table II. To improve the readability of the figure, the error bars on the $\Delta T_{ad}$ curves are displayed for the ternary compound, only.

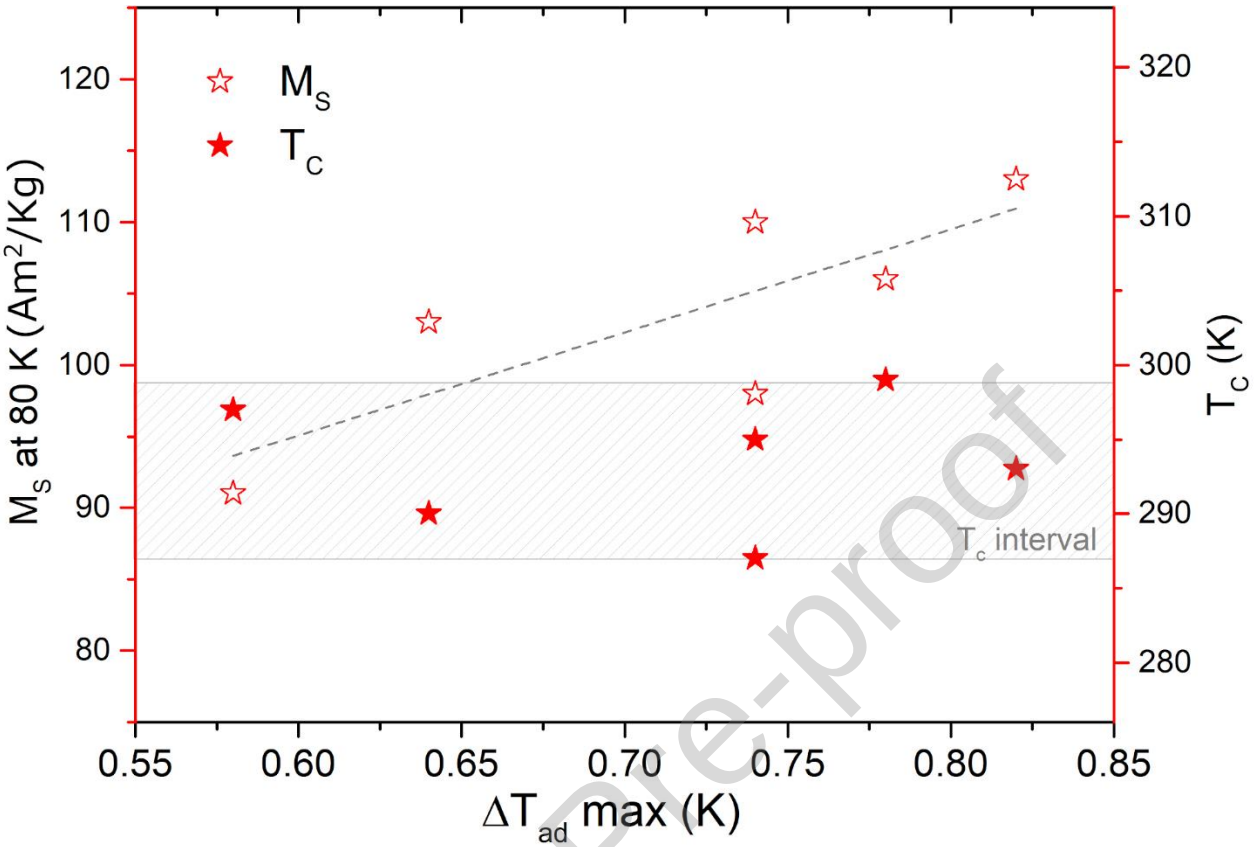


Figure 8: $\Delta T_{ad}^{max}$ measured for the quinary series and plotted as function of $M_S$ at 80K (left axis, hollow symbols) and $T_C$ (right axis, solid symbols).

# CRediT author statement

Simone Fabbrici Funding acquisition, Supervision, Conceptualization, Writing,
Francesco Cugini Investigation, Conceptualization, Writing
Fabio Orlandi Investigation
Nicola Sarzi Amadè Investigation
Francesca Casoli Investigation
Davide Calestani Investigation
Riccardo Cabassi Investigation
Greta Cavazzini Investigation
Lara Righi Investigation
Massimo Solzi Conceptualization, Supervision, Writing
Franca Albertini Conceptualization, Supervision, Writing

**Declaration of interests**

☒ The authors declare that they have no known competing financial interests or personal relationships that could have appeared to influence the work reported in this paper.

☐The authors declare the following financial interests/personal relationships which may be considered as potential competing interests:

## Highlights

- The magnetocaloric properties at the Curie transition of Ni2MnIn based Heusler compounds show promising values and complete reversibility.

- Adjusting the composition with either magnetic or non-magnetic atomic species allows for a precise tuning of the Curie temperature, which is important from the application point of view.

- Depending on the doping element and on the amount of it, unwanted secondary phases can be controlled by adjusting the heat treatments

- Time of flight neutron diffraction unveils the preferential occupancy of the different atomic species, which results to be dependent on the doping elements.